Available online at www.sciencedirect.com
ScienceDirect
Polymer 48 (2007) 2109–2123
polymer
www.elsevier.com/locate/polymer

Control the strain-induced crystallization of polyethylene terephthalate by temporally varying deformation rates: A mechano-optical study

Carla I. Martins, M. Cakmak*

Polymer Engineering Institute, Department of Polymer Engineering, The University of Akron, Akron OH 44325-0301, USA

Received 12 December 2006; received in revised form 3 February 2007; accepted 5 February 2007
Available online 15 February 2007

Abstract

The mechano-optical behavior of PET is, for the first time, investigated under temporally varying rates to influence the basic mechanisms of structural organization leading to strain-induced crystallization. For this purpose, four rate profiles, Linear, Sigmoidal, Logarithmic and Exponential, were chosen and films were stretched in Uniaxial Constrained Width mode using newly developed biaxial stretching machine. This machine allows real time direct measure of true stresses, strains, in-plane and out-of-plane birefringences during the deformation. Substantial differences in the mechano-optical behavior and resulting structural mechanism were observed in all of the chosen rate profiles. Linear profile, taken as a standard, yields three stress-optical regimes (SOR) during deformation. At early stages of deformation the birefringence remains linear with stress and material remains amorphous. This is designated as Regime I representing classical stress-optical behavior observed in large number of non-crystallizable polymers. In Regime II, a fast increase of birefringence accompanies formation of crystalline structure with establishment of long-range connected network. In the final Regime III birefringence levels off as the chains approach their finite extensibilities.

All three regimes observed in Linear profile are also observed in Logarithmic and Exponential cases. However, Sigmoidal deformation shows only the first two regimes even though the film was stretched to the same total engineering strain as applied to all profiles. Logarithmic profile was found to induce early strain crystallization leading to early development of strain hardening. Exponential profile on the other hand retards the formation of ''potentially constraining'' long-range physical networks. This allowed the development of higher birefringence and crystallinity levels using this mode. A logarithmic birefringence–work relationship with two distinct stages was found to apply to all temporally varying profiles.

Keywords: Strain-induced crystallization; Optical behavior; PET

1. Introduction

Polyethylene terephthalate (PET) is a polyester material of major commercial relevance due to its enhanced mechanical, thermal and barrier properties. These properties are greatly affected by the degree of orientation and crystallinity imparted during its processing. Uniaxial and biaxial deformations as well as post annealing stage play an important role in the development of structure and performance characteristics. Characterizations of these deformation processes are of extreme importance to understand and control the structural mechanisms taking place in wide range of processing operations including the tenter frame, double bubble film blowing and stretch blow molding processes. Many studies were conducted to investigate the effect of processing conditions and modes of deformation on the final properties of PET [1–9]. Of major importance is the phenomenon of stress-induced crystallization occurring during the material deformation, in order to provide better uniformity and dimensional stability of the film as it is directly associated with strain hardening that substantially helps develop thickness uniformity in these processes. However, the fast structural transition mechanisms taking place during this phenomenon are difficult to access without proper on-line characterization methods. In this regard, Synchrotron

* Corresponding author.
E-mail address: cakmak1@uakron.edu (M. Cakmak).

0032-3861/$ - see front matter © 2007 Elsevier Ltd. All rights reserved.
doi:10.1016/j.polymer.2007.02.029

X-ray diffraction techniques [10–12], on-line spectral birefringence techniques [13–15] and real time FTIR [16] have been used lately by different research groups.

Under deformation, PET shows strain hardening. As suggested by Salem [17,18] its deformation can be decomposed by two stages: (i) smooth increase of stress with rapid increase in the crystallinity of the material (up to 15% crystallinity); (ii) sharp increase of stress at almost constant crystallinity. A critical level of strain of 0.9, depending on the strain rate and temperature was suggested for significant crystallization to occur [19]. Tener [14] shows that an increase in strain rate promotes the increase of birefringence at all stages of deformation. In addition, the development of birefringence is observed prior to the strain hardening of the material. Blundell and coworkers [20–22] showed that when very fast rates are applied to the material (faster than the chain retraction motion), crystallization is delayed till the end of the stretching process. Moreover orientation is reduced when high temperatures or low rates are applied.

Gorlier et al. [19] and very recently Kawakami et al. [23,24] suggested a mechanism for the structural development of PET. According to the former, first there is the orientation of the molecules that starts interacting with each other resulting in the appearance of ordered entities (mesophase). When these entities become significant in number (nucleation stage) network is formed and strain hardening occurs. In order for crystallization to occur (growth), a minimum level of molecular relaxation is needed for the accommodation of the chains. Therefore if fast rates are applied crystallization takes place only after the deformation process. Kawakami et al. [23], on the other hand, proposed the formation of a mesophase that nucleates the formation of imperfect crystals, forming a network and causing strain hardening to occur. During this last stage, crystal growth, crystal perfection and crystal orientation follow as the strain increases. Many other authors evidenced the formation of the mesophase as a precursor of strain hardening in PET [10,25], PEN [26–28] and PET/PEN copolymers [29,30].

The stress-optical behavior of PET was investigated [31–34]. Hassan and Cakmak [15,32], for example, showed very recently the existence of a four-stage stress-optical behavior in PET stretched under Simultaneous Biaxial mode. The first stage obeys the linear stress-optical behavior with stress-optical constant of 5.8 GPa^{-1}; in the second stage the birefringence increases very fast with the formation of poorly ordered crystals believed to be the nodes of a physical network; in the third stage the birefringence begins to level off with further crystallization of the material; and in the fourth stage birefringence becomes nearly constant while stress continues to increase. This last stage was associated to the full extensibility of the chains and appears only at fast rates. Ito et al. [33] investigated the effect of drawing temperature and drawing rate on the stress–birefringence relationship of PET. Ryu et al. [34] showed that deviation from linearity is associated to the strain-induced crystallization of the material and that the stress-optical rule is invalid when very low temperatures (close to T_g) or very high rates are applied due to the contribution of glassy stress.

Most of the studies involving the relationship between processing–structure–properties are based on experiments performed at constant velocity [35], constant strain rate [5,36,37] or constant load [38], in different modes of deformation (uniaxial vs biaxial), etc. These methods are of much simple base as compared with the complexities of deformations and thermal histories at which the material is subjected in a real process. The present study aims to go one step further in the investigation of the deformation of PET films by applying different types of deformations to the material at temperatures above T_g. Comparison between Linear, Sigmoidal, Logarithmic and Exponential deformations is made in UCW mode of deformation. Each of the above non-linear profile applies a fast rate of deformation at different times. Logarithmic profile applies high rates at low strains, the Sigmoidal profile applies high rates at intermediate strains, and Exponential profile applies high rates at high strains. One of the key issues one would like to investigate is the relationship between orientation/relaxation and its implications on stress-induced crystallization. In other words, one would like to answer the question: Is there a non-linear stretching profile that will help accelerate the orientation, crystallization and crystalline perfection and thickness uniformity developed in the rubbery state stretching of PET films?

2. Experimental procedure

2.1. Material

Two commercial grades of PET films are used in this study. The films have intrinsic viscosity of 0.81 and 0.69 dl/g that correspond to M_n of 28,900 and 22,800, respectively. The former is designated by HPET and the latter by LPET. Both films were kindly provided by M&G Polymers Co. in cast amorphous forms with a thickness of 0.5 mm.

2.2. On-line birefringence and true mechanical behavior measurements

A modified Iwamoto biaxial stretching machine was used in this study to obtain measurements of true stress, true strain and in-plane and out-of-plane birefringences. The machine consists in a conventional biaxial stretching machine with an optical system, a vision system and a motor controller. Thus, not only the machine is able to acquire the forces being exerted in the material, but also acquires the true strain, through measurements of the displacement of a dot pattern printed in the center of the sample, and the changes in the retardation of the film at 0 and 45° at the geometric center of the sample. The changes in the thickness in the film, needed for calculations of the birefringence and true stress, are determined based on the X and Y strains assuming the incompressibility of the material, as follows: $L_{X0} \times L_{Y0} \times T_0 = L_{Xt} \times L_{Yt} \times T_t$, where L_{X0} and L_{Y0} are the original distances between the dots in X and Y directions, respectively; L_{Xt} and L_{Yt} are the X and Y distances between the dots during the deformation of the material, respectively; T_0 is the initial thickness of the sample measured with a thickness gage and T_t is the local thickness

of the sample to be determined. Details on the validity of the measurements can be found elsewhere [15,32]. The temporal evolution of the birefringence was determined at 546 nm (green light wavelength) as follows:

(i) in-plane birefringence, Δn_{12}:

$$\Delta n_{12} = \frac{R_0(t)}{T(t)} \tag{1}$$

(ii) out-of-plane birefringence, Δn_{23}, using Stein's equation [39]:

$$\Delta n_{23} = -\frac{1}{T(t)}\left[\frac{R_0(t) - R_\theta(t)\left(1 - \frac{\sin^2\theta}{\overline{n}^2}\right)^{1/2}}{\frac{\sin^2\theta}{\overline{n}^2}}\right] \tag{2}$$

(iii) out-of-plane birefringence, Δn_{13}:

$$\Delta n_{13} = \Delta n_{12} + \Delta n_{23} \tag{3}$$

R_0 and R_θ are the retardation at 0 and 45° (θ is the tilting angle), respectively, and $\overline{n}$ is the average refractive index of the material, which is 1.57 for PET [2].

A Labview based software was developed to control the machine, acquisition of data and data treatment, permitting the user to set any desired temperature, rates and modes of deformation. A particular feature of the machine is that it allows the input of any type of global deformation profile in addition to the modes of deformation traditionally practiced (UCW − Uniaxial Constrained Width, SIM − Simultaneous Biaxial, SEQ − Sequential Biaxial). Among others, the Logarithmic, Exponential and Sigmoidal global deformations were investigated in this study and compared with the Linear deformation (constant speed). The above-mentioned programmed deformation profiles were input and the machine follows these profiles imposing global deformation. The actual true strains were determined from the image analysis of the prepainted dot matrix in the center of the sample. In this paper the engineering strains are the global engineering strains based on gage separation. True strains are local true strains determined by high speed CCD coupled with automated image analysis system. In-plane and out-of-plane birefringences are measured in geometric center of the sample at one spot where true strains are also determined through image analysis system. True stress is calculated based on the load cell force reading on one of the grips on each side that is divided by the instantaneous thickness calculated in the center of the sample.

2.3. Sample preparation and experimental conditions

Samples of 14 × 14 cm were cut from the as cast films, where an array of 24 dots was printed. The machine was pre-warmed up to 85 °C for a period of at least 2 h prior to the stretching process. The samples were then placed and clamped in pneumatic clamps for additional 8 min for thermal equilibration prior to start of deformation. The samples were stretched in the Uniaxial Constrained Width (UCW) mode, with the following types of deformation: (i) Linear, (ii) Sigmoidal, (iii) Logarithmic and (iv) Exponential profiles. These profiles are represented in Fig. 1. The total time of the experiment in each profile was kept constant based on a time needed to stretch the sample in the linear mode, at a constant speed of 1.5 mm/s (0.0125 s^{-1}) to a total stretch ratio of 3.5 × 1. The following stretch ratios $\lambda_{MD} \times \lambda_{TD}$ were used: 1.5 × 1, 2 × 1, 2.5 × 1, 3 × 1, 3.5 × 1. After stretching, the films were immediately cooled to temperatures below its glass transition by fans integrated in the machine and an external fan directed to the center of the sample. During this process the sample was held constrained by the clamps.

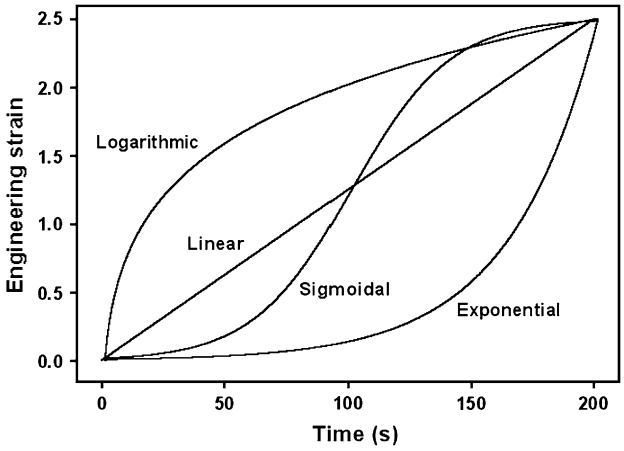

Fig. 1. Types of deformation applied to PET: engineering strain vs time (global deformation history).

2.4. Thermal characterization

Thermal properties of PET films were measured using a 2920 MDSC V2.6A TA instruments. The samples of approximately 6–10 mg were scanned between 25 and 300 °C at the heating rate of 20 °C/min in a dry nitrogen atmosphere. The thermal properties are referred to the midpoint in the case of T_g and to the maximum peak position, in the case of T_{cc} (cold crystallization temperature) and T_m (melting temperature). The degree of crystallinity was determined using Eq. (1), considering the heat of fusion of 100% crystalline (ΔH_f^0) PET to be 120 J/g [40].

$$\chi(\%) = \frac{(\Delta H_m - \Delta H_c)}{\Delta H_f^0} \times 100 \tag{4}$$

ΔH_m and ΔH_c are, respectively, the enthalpy of melting and enthalpy of crystallization.

The thermal properties of the initially amorphous PET films (less than 5% crystallinity) are presented in Table 1.

Table 1
Thermal properties of amorphous PET

	T_g (°C)	T_{cc} (°C)	T_m (°C)
LPET	73.3	132.6	253.5
HPET	75.5	136.5	252.6

2.5. X-ray measurements

Bruker AXS Generator equipped with a copper target tube and two-dimensional detector was used to obtain the one-quadrant of WAXD patterns of the specimens. The generator was operated at 40 kV and 40 mA with a beam monochromatized to Cu Kα radiation. The sample to detector distance was kept at 11.5 cm. A typical exposure time of 15 min was used.

3. Results

3.1. Strain measurements

In Fig. 2, the true Hencky strain and engineering strain are compared for each type of deformation applied.

In all cases the engineering strain that is imposed by the programmed profile overestimates the strains occurring locally at the center of the sample. The gap between the two measures widens at large deformations. In addition, while engineering strain predicts no deformation in the transverse direction (TD), the calculation of the true Hencky strain based on the movement of the dot pattern shows a negative strain occurring in the sample in this direction indicating some degree of retraction that is taking place in TD while MD stretching proceeds. Measurements based on gage separation cannot detect this natural deformation behavior of films.

3.2. Strain rate measurements

The change of strain rate in the material during the total period of the stretching is represented in Fig. 3 for each type of deformation profile. In the Linear case, the strain rate initially set at 0.0125 s^{-1} gradually decreases with time. In the Logarithmic deformation, although the strain rate is very high at the beginning, it decreases very rapidly to values below 0.0125 s^{-1} in the first 30 s, slowly decreasing thereafter until it reaches zero at the end of the stretching process. In the Sigmoidal case, the strain rate increases slowly to a maximum around 100 s. Beyond this time it decreases until the end of the stretching process. The strain rate applied at intermediate times is higher than the strain applied in the Linear case. For the Exponential deformation function selected for this experiment, the strain rate increases exponentially till around 185 s, time at which it starts to decrease.

In many processes some of these non-linear rate profiles naturally occur. For example the Sigmoidal deformation profiles are observed during the tubular film bubble inflation [41]. A logarithmic type of profile can also be found in this process [42]. Theoretical analysis on the film casting deformation predicts also an increase of strain rate similar to the one observed for Sigmoidal deformation, till its maximum is reached [43].

In Figs. 4 and 5 the Hencky strain rate is plotted as a function of the Hencky strain for LPET and HPET, respectively, in

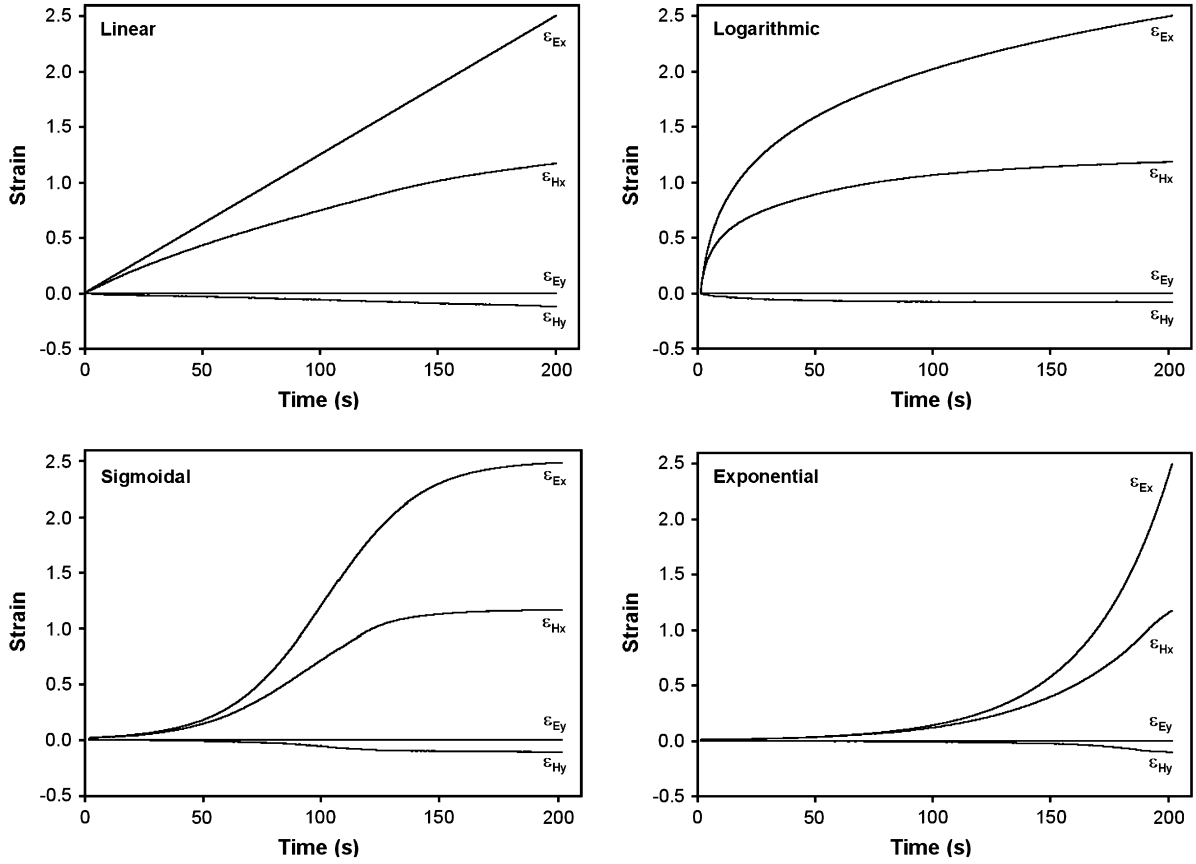

Fig. 2. Comparison between engineering strain (ε_E) (global) and true Hencky strain (ε_H) (local) for the different types of deformations.

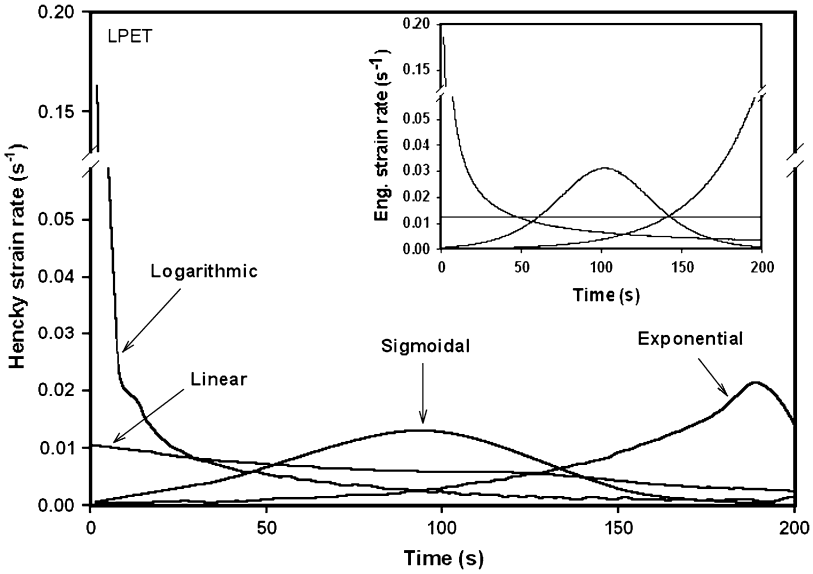

Fig. 3. Hencky strain rate as a function of time and type of deformation applied for LPET stretched at 85 °C. In insert: engineering strain rate as a function of time.

order to map the deformation rates onto strains occurring throughout the deformation. This also helps to eliminate the time factor, as the speed is non-linear in these profiles except in the linear one.

The results show that both HPET and LPET are subjected to identical strain rates when Linear, Sigmoidal and Exponential deformations are applied. In the case of Logarithmic deformation, the strain rate of LPET is much higher than the strain rate of HPET, for the same strain level. In both M_w materials, the strain rate of the Logarithmic profile is much higher than any of the other deformations. Only at 60% strains the strain rate reaches the same level of the other types of deformation. At 100% it is observed that the strain rate has decayed to a zero strain rate, in the case of HPET.

The strain rate applied to the material during a Sigmoidal deformation shows a plateau that lasts from around 20 to 90% strains. Therefore, the deformation of the material takes place mostly at constant strain rate even though the externally applied profile is highly non-linear sigmoidal shape.

3.3. Optical behavior

The temporal change of in-plane and out-of-plane birefringences for each type of deformation studied is represented in Fig. 6. For all deformations, Δn_{12} and Δn_{13} increase significantly, whereas Δn_{23} shows only a small increase. These results are expected due to the orientation of the chains in the stretching direction, which increases the refractive index of the film in the MD (n_1) and at the same time it decreases the refractive index in the ND (n_3) due to the realignment of the phenyl group parallel to the surface of the film [44]. The refractive index of the TD (n_2) is also expected to decrease [45], but at less extent than the ND, and therefore there is a small positive increase of Δn_{23}.

The temporal development of birefringence generally follows the imposed deformation profile. In the Linear deformation, the birefringence increases throughout the deformation and it accelerates beyond 120 s. In the Logarithmic deformation,

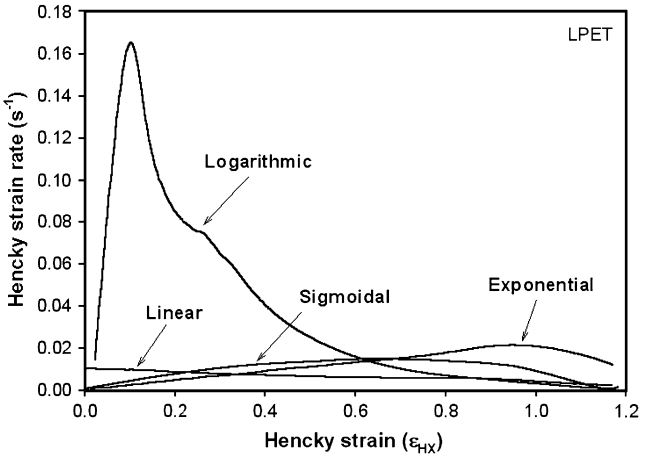

Fig. 4. Hencky strain rate as a function of Hencky strain and type of deformation applied for LPET stretched at 85 °C.

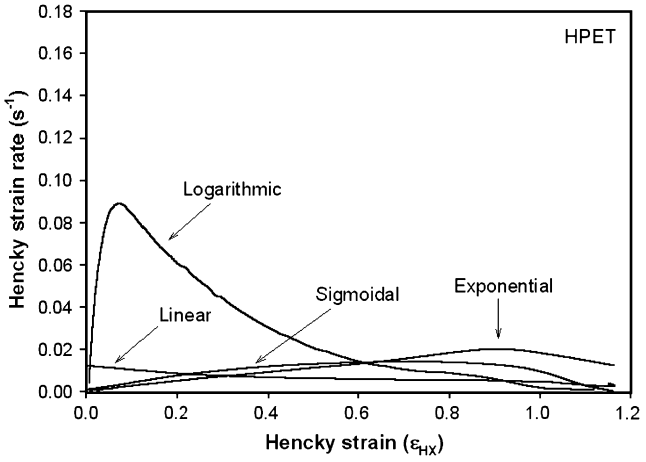

Fig. 5. Hencky strain rate as a function of Hencky strain and type of deformation applied for HPET stretched at 85 °C.

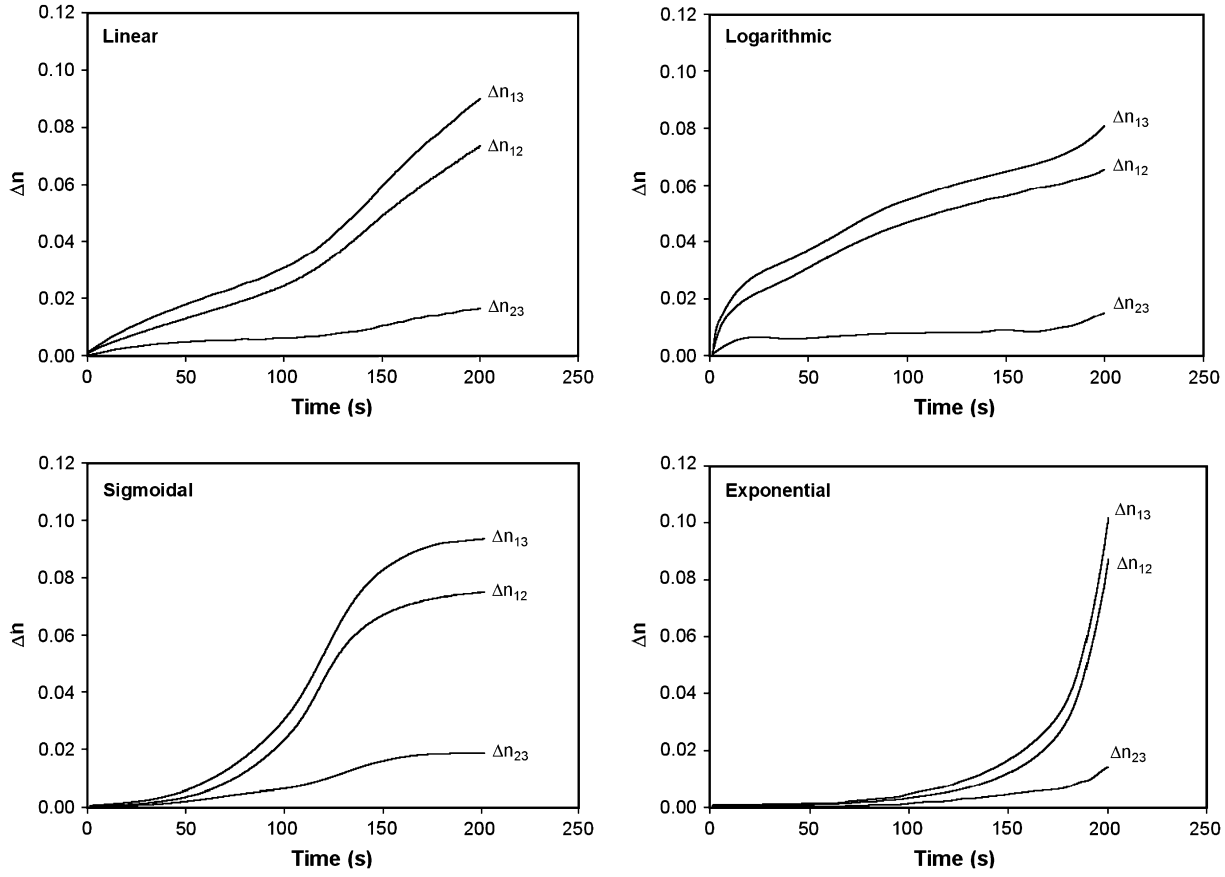

Fig. 6. Optical behavior of LPET as a function of type of deformation.

there is a very fast increase in the birefringence at low times, which then slows down showing a shoulder and started increasing at much slower rate. The Sigmoidal deformation shows a fast increase of birefringence at intermediate times, leveling off above 150 s. This result contrasts with the Logarithmic profile in the sense that for long times both of them have little deformation occurring locally in the material (see Fig. 2) and while the Logarithmic deformation shows an increase of birefringence all the time, in the Sigmoidal case it is almost zero after 150 s. This result might show some mechanistic differences in the orientation and structural development of the material. In the last case of Exponential deformation, the birefringence starts increasing only above 100 s, increasing very rapidly thereafter, accompanying the deformation applied. Among all, the Exponential deformation is the one that shows higher final in-plane and out-of-plane birefringences, followed by the Sigmoidal, Linear and Logarithmic deformations. If one compares the changes of strain rate with the slopes of birefringence change for each type of deformation, it is observed that at low times, the slope is higher in the following order: Logarithmic, Linear, Sigmoidal and Exponential, whereas at long times, the slope is higher for Exponential, Sigmoidal, Linear and Logarithmic. This change in tendency correlates well with the changes in strain rate plotted in Fig. 3. Just as example, the Logarithmic strain rate is the highest at low times and is the lowest at long times, causing therefore a very fast increase of birefringence at first that slows down thereafter.

3.4. Mechanical behavior

The mechanical behavior of LPET and HPET is shown in Fig. 7 and Fig. 8, respectively. Upon deformation, an expected increase of stress in the MD (σ_{11}) is accompanied by a small increase of stress in the TD (σ_{22}). The films naturally contract in the transverse direction when MD stretching is applied (Fig. 2). These data reflect this behavior.

For LPET, Linear, Sigmoidal and Exponential deformations have the same mechanical response at low strains, where σ_{11} increases nearly linearly with the increase of strain. For HPET, the Sigmoidal and Exponential deformations have the lowest stresses at low strains, crossing over the Linear deformation at a Hencky strain of 40%. With the increase of strain, the difference in stress level for each type of deformation becomes larger. They order as: Exponential > Sigmoidal > Linear > Logarithmic. In both M_w materials, the stress increase tends to slow down reaching a quasi plateau just prior to the strain hardening.

The behavior observed in the Logarithmic profile is different as compared to the other profiles. In this case, there is a very fast rise of the stress at low strains, as a result of the high rates applied to the material. Other authors have shown this behavior when PET is deformed at very high rates or temperatures close to the T_g [34]. The stress keeps increasing until it reaches a plateau and then strain hardens. The plateau in the Logarithmic case is longer and appears at lower stresses when compared to the other profiles. This result shows that

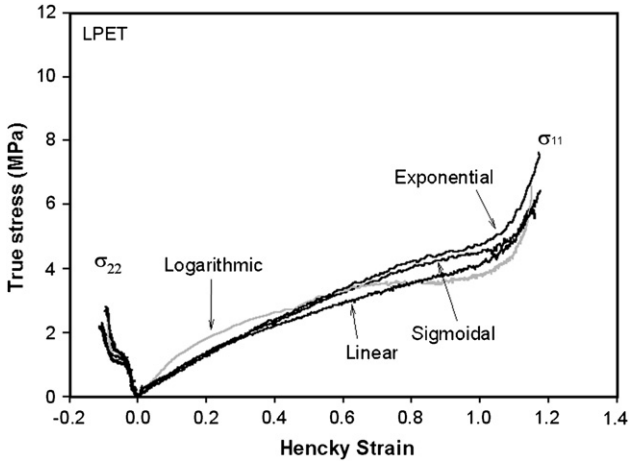

Fig. 7. True mechanical behavior of LPET stretched with different types of deformation profiles, in UCW mode at 85 °C.

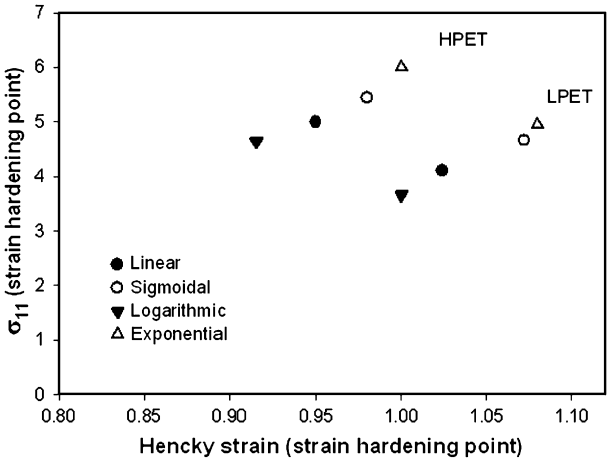

Fig. 9. Effect of deformation profile on the critical true stress and critical true strain at the strain hardening point of LPET and HPET.

significant relaxation might take place simultaneously to the orientation of the material, as a result of the substantial reduction in the strain rate applied observed above 60% strains (see Figs. 4 and 5). It should be emphasized that the onset of strain hardening shifts to lower strains and lower stresses in Logarithmic profile as compared to others. This result is shown in Fig. 9. Strain hardening is quite significant in controlling the thickness uniformity of the films. The lower the strain hardening the lower the strains at which the "self leveling" can take place in these films [6]. All the deformation profiles investigated show strain hardening of the material starting from 90 to 100% strains. This value is in good agreement with the observed value by Gorlier et al. [19]. Strain hardening is more pronounced for HPET than LPET as expected from increased entanglement density in longer chains that accelerate the orientation development and consequent strain-induced crystallization and strain hardening.

3.5. Mechanical–optical behavior

In Figs. 10 and 11, the in-plane mechano-optical behavior – Δn_{12} vs $(\sigma_{11} - \sigma_{22})$ – of LPET and HPET is shown for all the deformation profiles. Three regimes are distinguished: Regime I, where stress-optical rule applies, with a stress-optical constant of 8 GPa^{-1}. The SOC is slightly higher than that previously reported by some authors [15,34,46,47], however, according to Ajji and Zhang [48] it can vary between 3.8 and 8 GPa^{-1}. Regime I is independent of M_w and of the type of deformation applied. Sigmoidal and Exponential deformations cause an extension of the linear region, associated with Regime I, to higher stresses and birefringences, as compared to the Logarithmic and Linear deformations.

Regime II is characterized by a fast increase of birefringence with small increase of stresses. This regime is greatly affected by the types of deformation applied. For example, the slope of Regime II becomes more abrupt as one changes from Linear, Exponential and Sigmoid deformations, becoming even negative in the case of Logarithmic deformation. The transition from Regime I to Regime II occurs in the following order: Logarithmic, Linear, Sigmoidal and Exponential, suggesting that earlier application of high rates leads to earlier transition. Regime II is also considerably longer for all the other deformations as compared to the Linear one,

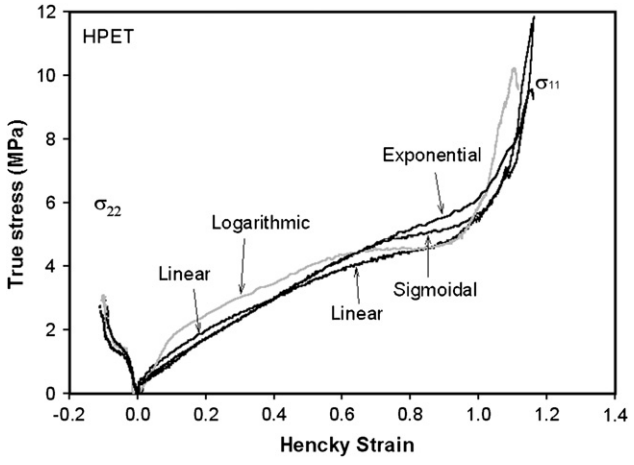

Fig. 8. True mechanical behavior of HPET stretched with different types of deformation profiles, in UCW mode at 85 °C.

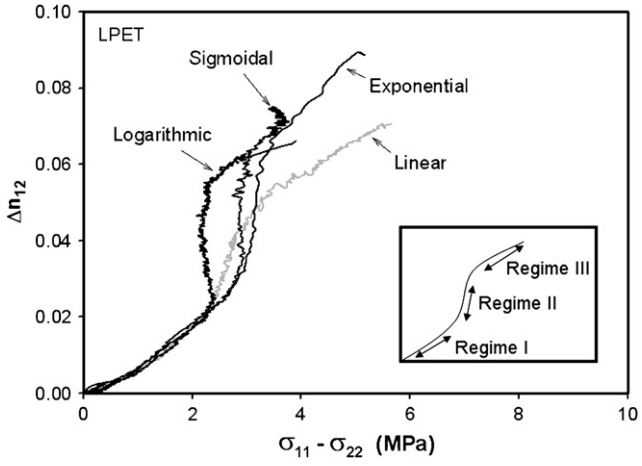

Fig. 10. In-plane mechano-optical behavior of LPET stretched with different types of deformation profiles, in UCW mode at 85 °C.

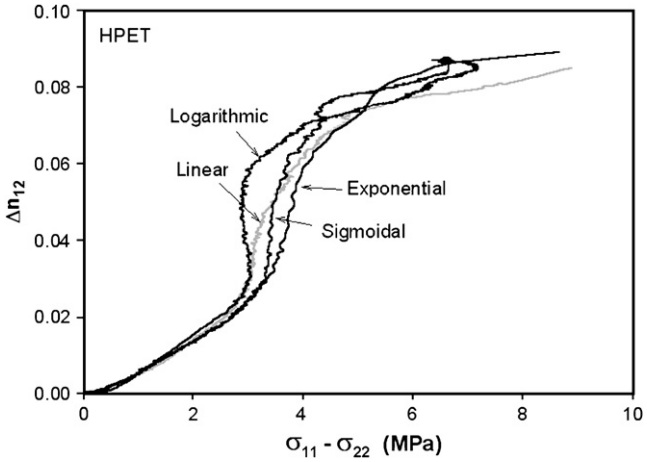

Fig. 11. In-plane mechano-optical behavior of HPET stretched with different types of deformation profiles, in UCW mode at 85 °C.

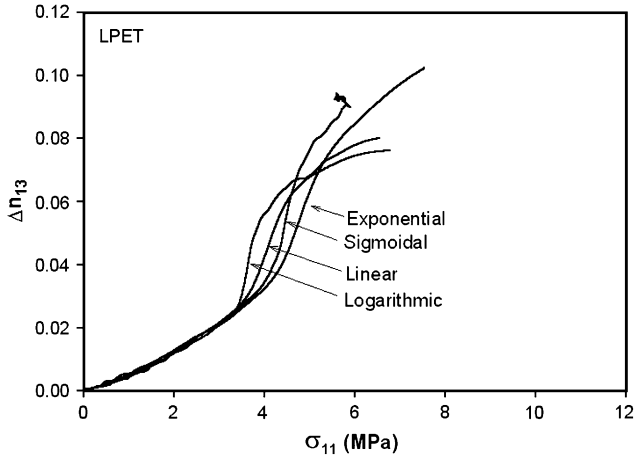

Fig. 12. Out-of-plane mechano-optical behavior of LPET stretched with different types of deformation profiles, in UCW mode at 85 °C.

indicating that much higher orientation is achieved for the same level of stress. This behavior is more pronounced in the case of LPET than HPET.

Regime III shows a strong dependency on the M_w and on the type of deformation applied, i.e. much bigger differences are found between the deformation profiles in LPET than HPET. This behavior is due to the differences in the strain hardening of the two M_w materials, as shown in Figs. 7 and 8. In general, Regime III occurs when maximum extensibility of the chains is achieved that tightens the network and causes the stress to rise. Thus, the increase of stress is only accompanied by small increases of birefringence. This behavior is seen in the case of HPET where the birefringence levels off around 0.08 while the stress increases and not in LPET. This result seems to indicate that the mechanism of network tightening is more significant for HPET than for LPET. This behavior is in line with the expectations as the longer chains should form long-range network connectivity at lower deformation levels due to multiple factors including reduction of orientation relaxation rates and faster stress build-up.

For LPET, the Logarithmic and Sigmoidal deformations have a very short Regime III, indicating that considerable chain relaxation is taking place simultaneously to the deformation process, preventing the stress to build up. This phenomenon can be understood simply by the fact that the deformation rate decreases in both cases at the end of deformation process, allowing the molecular relaxation to dominate over the orientation process. The orientation/relaxation phenomenon is well documented in the literature for deformation at constant speed (Linear deformation), being more pronounced at lower deformation rates [21]. In the particular case of Sigmoidal deformation, a small relaxation stage is clearly observed at the end of Regime III, showing that molecular relaxation becomes more significant than the molecular orientation. This behavior is also seen in the Sigmoidal and Logarithmic cases of HPET. Exponential deformation induces a substantial increase of birefringence as compared to all the other cases together with an increase of the stresses.

The out-of-plane mechano-optical behavior – Δn_{13} vs σ_{11} – is plotted in Figs. 12 and 13, respectively, for LPET and HPET. The behavior is very similar to the in-plane mechano-optical behavior, with the exception of the SOC. In this case the SOR is 6 GPa^{-1} which is lower than the previous one.

Fig. 14 shows the in-plane mechano-optical behavior of LPET with correspondent time slicing, aiming to answer the following question: why is the linear stress-optical region extended to higher stresses for Sigmoidal and Exponential deformations, when those start at lower rates than Linear and Logarithmic deformations? According to previous observations [15,33,34] the SOR is extended as the rate of deformation increases.

If one compares Fig. 1 or Fig. 3 with Fig. 14, it is observed for example that for a Sigmoidal deformation, the strain starts to increase more rapidly after 50 s. For the same time, only a very small increase in the birefringence and stress is observed. Thus once the rapid deformation stage starts, it leads to an extension of Regime I just as it has been observed in high speed stretching conditions in constant speed stretching experiments. The same happens with the Exponential deformation, as it is seen by the comparison of the same Figures at 100 s.

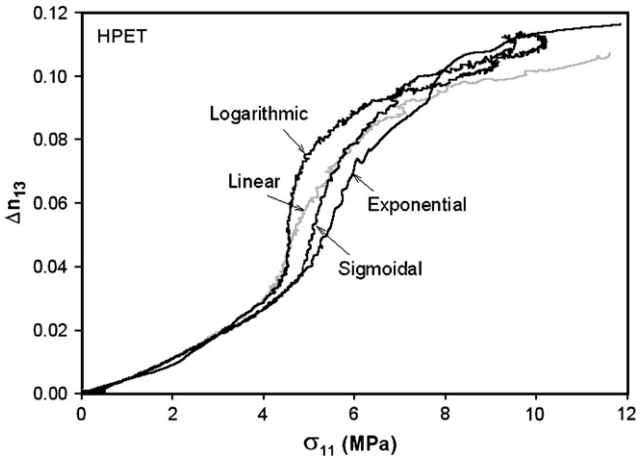

Fig. 13. Out-of-plane mechano-optical behavior of HPET stretched with different types of deformation profiles, in UCW mode at 85 °C.

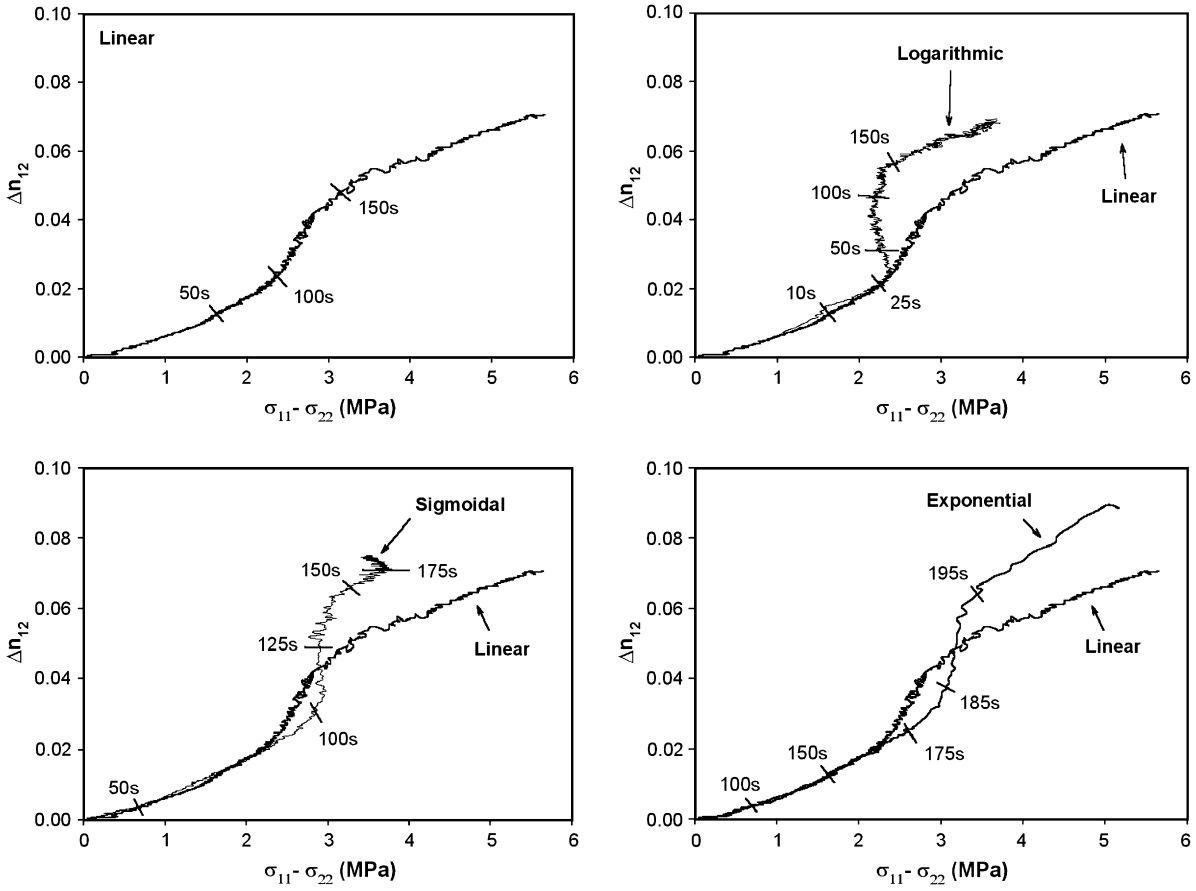

Fig. 14. Time slicing of mechano-optical behavior of LPET for each type of deformation profile.

The Logarithmic deformation, on the other hand, should show an extension of the Regime I. Since the rates are so fast at the early stages of deformation, 25 s are enough to cause an increase in the birefringence and stress much higher than any other type of deformation. Nevertheless, the strain rate has substantially decreased at this time giving the possibility for the molecules to start relaxing and thus crystallize more rapidly, causing the deviation from linearity of SOR to occur at this instant. This behavior is confirmed by the results shown in Fig. 15. For the Logarithmic deformation a very fast increase of crystallinity is observed at lower stresses as compared to any other type of deformation. This behavior is augmented in the case of HPET. Blundell et al. [21] shows that when PET is deformed at very fast rates, crystallization takes place only when the process of deformation stops. A similar mechanism seems to be occurring in the Logarithmic case, although in here one needs to think that the deceleration in the rate of deformation also helps on the fast crystallization of the material. Mulligan [49] also observed similar behavior for PLA, but since the molecular chains of PLA are much longer than PET it takes some time to crystallize. Forced small strain retraction experiments have shown to instantaneously enhance crystallization of PLA.

The comparison between the types of deformation shows that till $(\sigma_{11} - \sigma_{22})$ of 2 MPa, the crystallinity increases slightly and for the same amount in all the deformation profiles. LPET shows higher level of crystallinity at this point. With a small increase of stresses, for example $(\sigma_{11} - \sigma_{22})$ of 2.5 MPa, the increase of crystallinity becomes greatly dependent on the type of deformation. Exponential and Sigmoidal deformations show a small increase of crystallinity (12–15%), whereas Logarithmic have a considerable increase to about 28% in both materials. Further increase of stress shows a rapid increase of crystallinity in LPET for the Exponential and Sigmoidal deformations that is much higher than in the Linear deformation. Logarithmic deformation profile, on the other hand, shows only a 2% increase in the crystallinity of the material. HPET have a different behavior, since above $(\sigma_{11} - \sigma_{22})$ of 4 MPa, the percentage of crystallinity becomes almost independent of the deformation type, leveling off around 30% crystallinity (on average). Among all, the Linear deformation shows the lowest percentage of crystallinity.

To detail the structural mechanisms occurring for each type of deformation, the in-plane mechano-optical behavior is shown with correspondent WAXD patterns and percentage of crystallinity as measured by DSC. This is represented in Figs. 16–19, respectively for Linear, Sigmoidal, Exponential and Logarithmic deformations.

All the profiles have similar behavior in Regime I, as described before. In this regime, till about $(\sigma_{11} - \sigma_{22})$ of 2 MPa, the WAXD pattern shows the appearance of a broad halo, correspondent to an amorphous structure and, as indicated

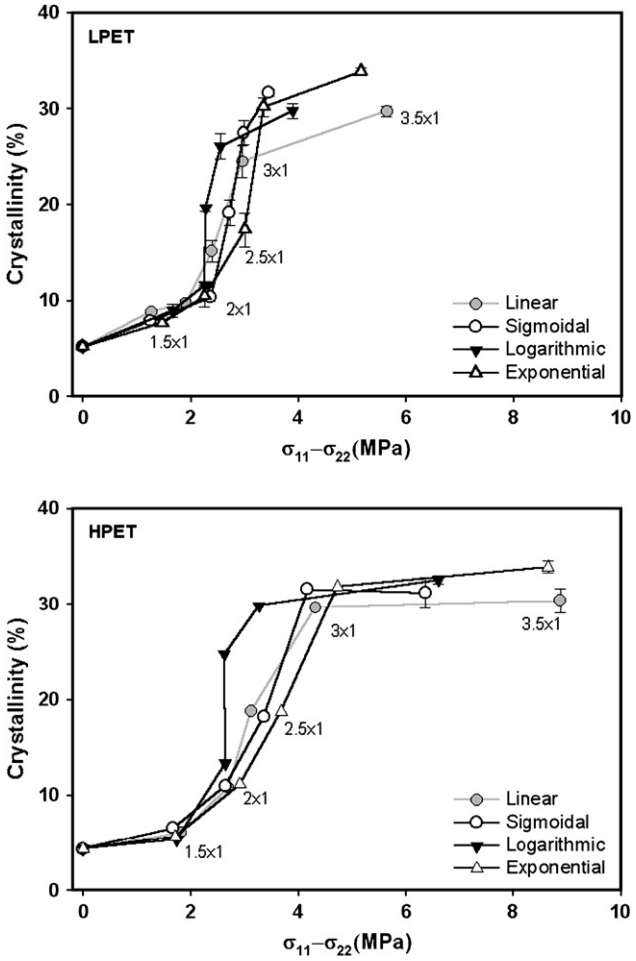

Fig. 15. Crystallinity of LPET and HPET as a function of stress difference: effect of type of deformation.

by the DSC measurements, the percentage of crystallinity has increased only slightly. When deviation from linearity occurs, in the transition from Regime I to II, an increase in the percentage of crystallinity is observed, that is dependent on the type of deformation applied, as discussed previously. The WAXD pattern in this case shows a concentration of the amorphous halo in the equatorial region indicating the development of preferentially oriented amorphous chains in the machine direction. In Sigmoidal profile, the WAXD pattern begins to show faint equatorial peaks starting when Δ_{12} reaches 0.03.

During Regime II, the birefringence increases very rapidly as a result of the fast rise in the crystallinity of the material. Depending on the deformation profile, the crystallinity can increase to more than 25% at the end of this stage. The higher orientation achieved with either Logarithmic or Exponential deformations, results in the appearance of very clear peaks in the WAXD pattern in the middle of Regime II (Δ_{12} around 0.04). These peaks become more pronounced as the Regime III develops.

In Regime III, the birefringence keeps increasing while the stress rises as a result of strain hardening, especially in the Exponential case. However, only a slight increase in the percentage of crystallinity is observed for all the types of deformation in this stage indicating that overall structure is reaching a saturation level. This result indicates that the Exponential deformation profile promotes higher birefringence development with further alignment of the amorphous chains. This can occur if the long-range network formation is retarded to higher deformation levels allowing further alignment of the polymer chains. Evidences of this behavior are also shown by the increase in the T_g of the material at $(\sigma_{11} - \sigma_{22})$ above 3 MPa, maintaining the maximum peak of T_{cc} at the same constant temperature. These results are shown in Fig. 20.

3.6. Strain-optical behavior

The strain-optical behavior of LPET and HPET is plotted in Fig. 21. The birefringence increases nearly linearly as the

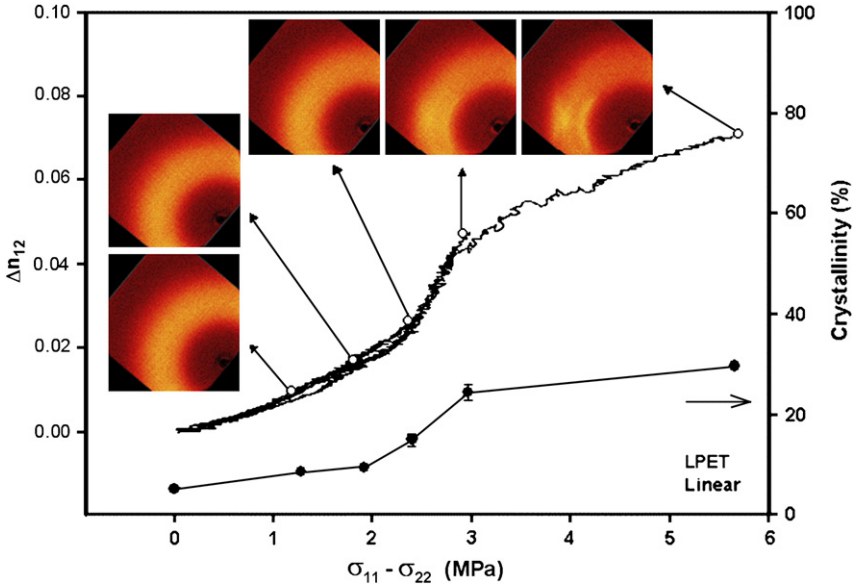

Fig. 16. In-plane mechano-optical behavior of LPET subjected to a Linear deformation with respective WAXD patterns and % crystallinity.

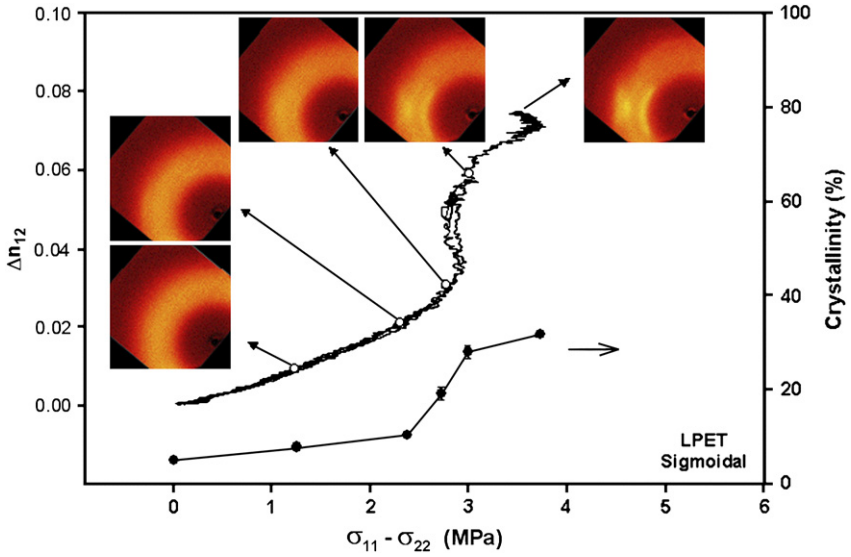

Fig. 17. In-plane mechano-optical behavior of LPET subjected to Sigmoidal deformation with respective WAXD patterns and % crystallinity.

strain increases. Beyond strains of 70%, the slope increases over a relatively broad range. This point coincides to the transition from Regime I to Regime II of the stress-optical rule discussed above. Only a small dependency on the type of deformation is observed in contrast to the stress-optical behavior.

At lower strains the Logarithmic profile shows higher birefringence for the same strain as compared to all other profiles signifying its effectiveness in influencing the orientation behavior at early stages of deformation. This effect is more pronounced in HPET. The influence of molecular weight becomes quite substantial, particularly at high strains where the birefringence is higher in HPET. During Regime I, Logarithmic deformation shows the larger increase of birefringence, whereas the Exponential shows the smallest one. When the material enters in the Regime II, this tendency changes and Exponential deformation is the one causing the higher increase of birefringence, especially for LPET. HPET does not seem to be affected. As prescribed in the deformation profile, a cross-over between the Logarithmic and the rest of the profiles were observed especially in LPET data. This points to the domination of relaxation processes in the Logarithmic profile over orientation processes at large strains.

The strain-optical behavior of PET is presented in appendix as: (a) the change of birefringence as a function of exponential of true strain (Δn vs $\exp(\varepsilon)$) and as (b) the change of birefringence as a function of exponential of the double of the true strain (Δn vs $\exp(2\varepsilon)$).

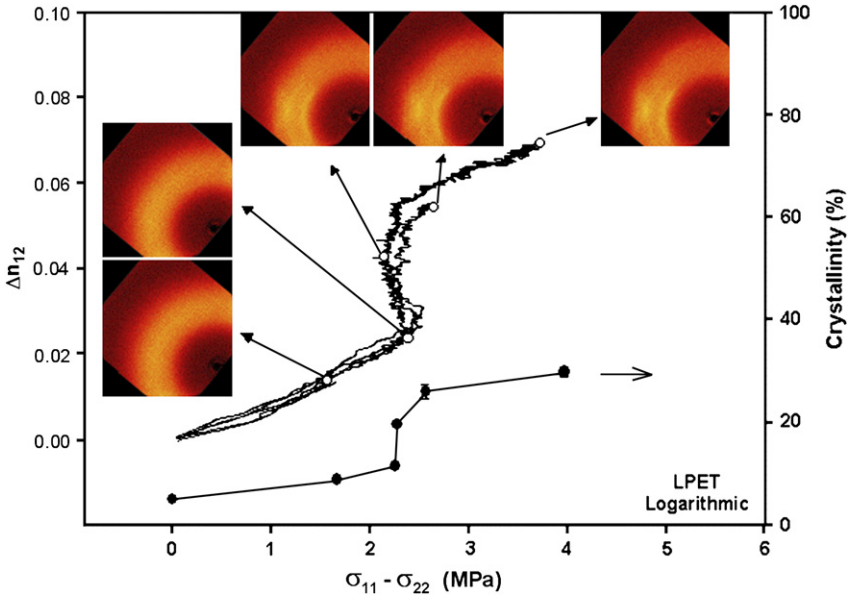

Fig. 18. In-plane mechano-optical behavior of LPET subjected to Logarithmic deformation with respective WAXD patterns and % crystallinity.

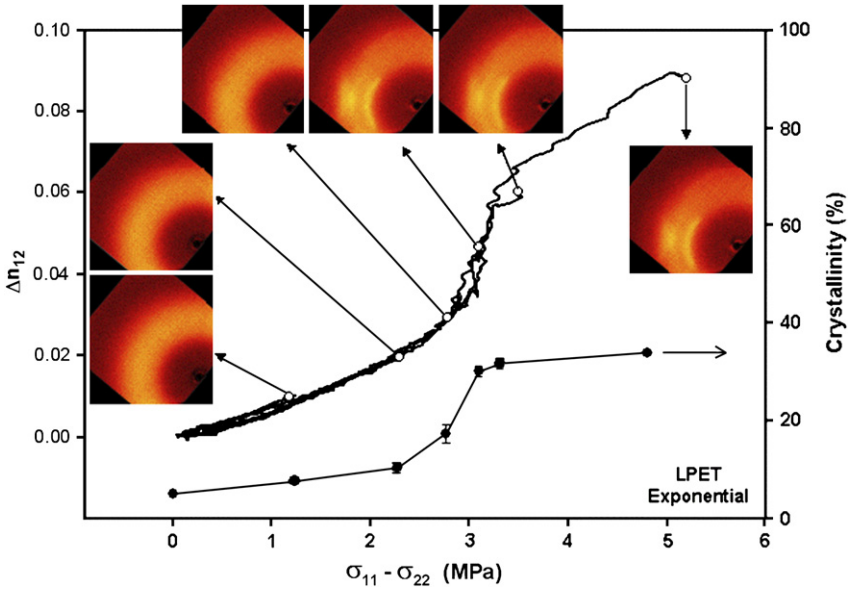

Fig. 19. In-plane mechano-optical behavior of LPET subjected to Exponential deformation with respective WAXD patterns and % crystallinity.

The percentage of crystallinity of LPET and HPET as a function of Hencky strain in plotted in Fig. 22. Both M_w materials have a distinct behavior from each other regarding the effect of the type of deformation. In the case of LPET there is a small but linear increase of crystallinity at strains below 60%. Logarithmic deformation shows a slightly higher crystallinity than the other profiles indicating that the strain-induced crystallization is accelerated with the use of high speeds early in the Logarithmic profile.

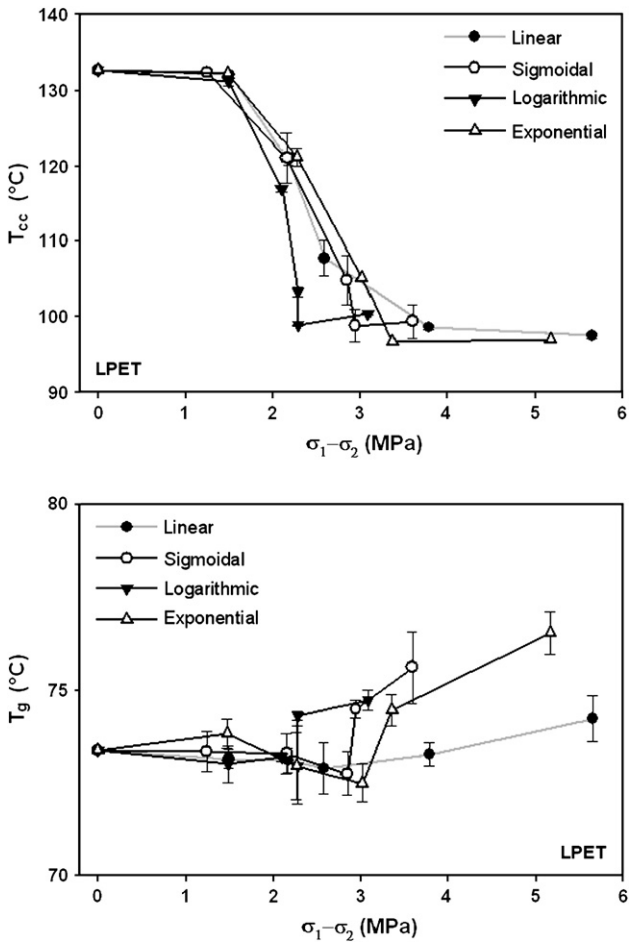

Fig. 20. Change in the thermal properties of LPET with the different types of deformation.

In the Exponential profile the lowest increase is observed as this profile applies the lowest rate at the early stages of deformation. As the strain increases further, the % of crystallinity starts to increase faster, becoming more dependent on the type of deformation. At strains around 80%, the percentage of crystallinity is around 18% for the Logarithmic, Exponential and Sigmoidal, whereas for Linear is around 15%. This critical strain marks the point at which the Logarithmic profile is no longer the type of deformation imparting higher % of crystallinity in the material, changing it for the Exponential and Sigmoidal cases. As the strain increases, the Exponential deformation leads to higher % of crystallinity, followed by the Sigmoidal deformation. The Logarithmic deformation tends to stabilize at a value similar to the linear one at high strains. A difference of 6% in the crystallinity of the material is observed between the Linear and Exponential cases, at 100% strains.

For HPET, crystallinity starts increasing above 40% strains, exhibiting a clear distinction for the Logarithmic as compared to the other profiles. A faster increase in the % of crystallinity is always observed till strains slightly above 100%. At this strain level, the % crystallinity is identical for all types of deformation and starts increasing more rapidly for the Exponential case, as the strain increases.

By comparing the behavior of the two M_w materials, it is observed that at strains of 40%, LPET has higher % of crystallinity than HPET, as a result of the higher strain rate applied to the material, as observed in Figs. 4 and 5. At strain between 60 and approximately 100%, the % of crystallinity is higher only for the Logarithmic deformation of HPET, maintaining the same value at all the other deformations in both M_w's. At

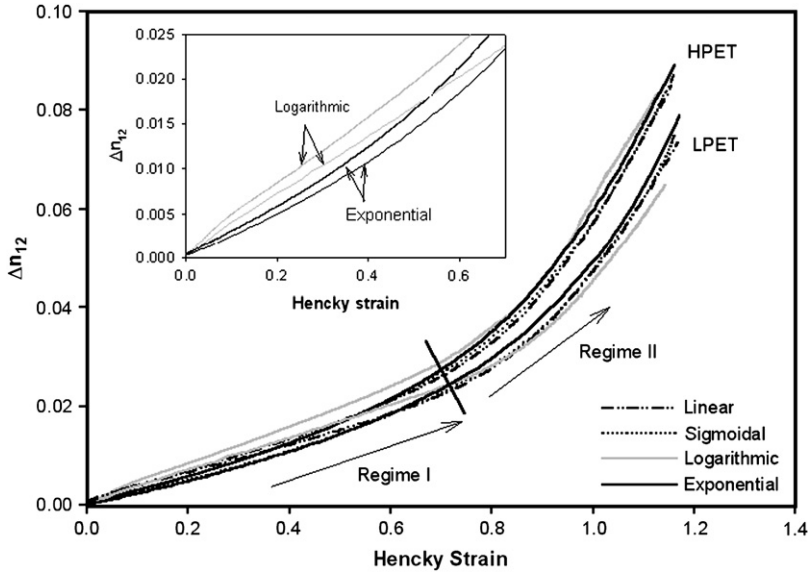

Fig. 21. Strain-optical behavior of PET as a function of M_w and type of deformation.

100% strains HPET shows the same value of crystallinity independently of the type of deformation, whereas LPET is dependent on the deformation profile.

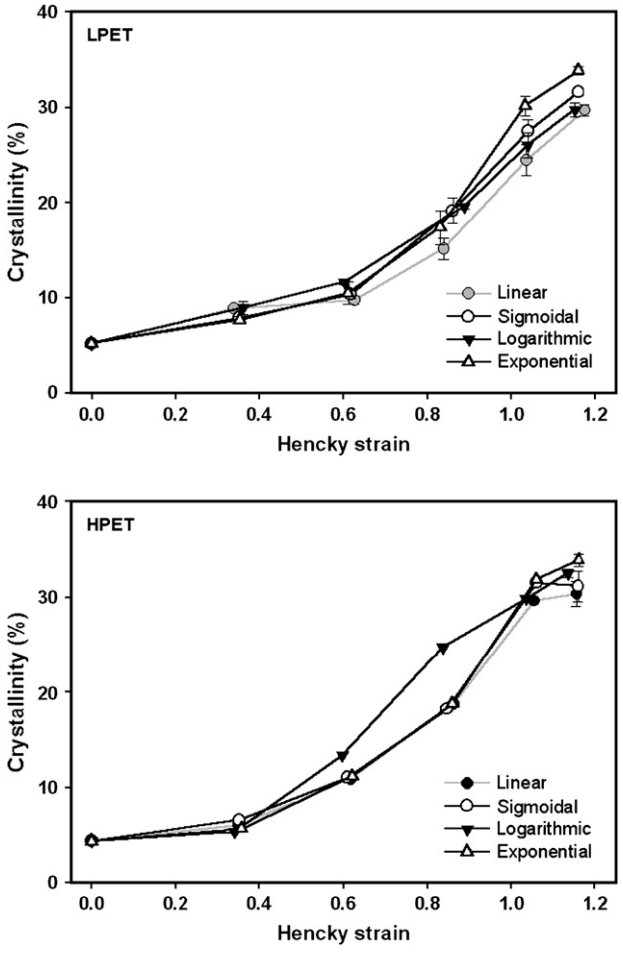

Fig. 22. Crystallinity of LPET and HPET as a function of Hencky strain: effect of type of deformation.

3.7. Work-optical behavior

Fig. 23 shows the work-optical relationship for the two M_w materials and types of deformation applied. The total work inputted in the material was determined from the following relationship:

$$W_T = \int_0^t \underline{\underline{\sigma}} : \underline{\underline{D}}\, dt \tag{5}$$

where $\underline{\underline{\sigma}}$ is the stress tensor and $\underline{\underline{D}}$ is the deformation rate tensor. In the case of Uniaxial Constrained Width, the total work is defined as follows:

$$W_T = \int_0^t \left(\sigma_{11}\dot{\varepsilon}_{11} + \sigma_{22}\dot{\varepsilon}_{22}\right) dt \tag{6}$$

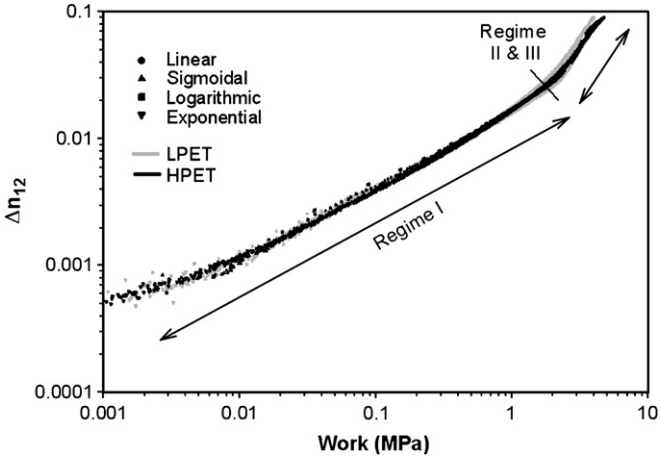

Fig. 23. Work-optical behavior of PET as a function of M_w and type of deformation.

where σ_{11} and σ_{22} are the true stresses in MD and TD, respectively, and $\dot{\varepsilon}_{11}$ and $\dot{\varepsilon}_{22}$ are the strain rates also in the MD and TD, respectively.

In a double log plot the relationship between birefringence and work is an independent function of the type of deformation and M_w of the material. There is a two stage linear relationship between $\log \Delta n_{12}$ and $\log w$. In both of them the birefringence increases with the work applied to the material, which is faster in the second stage. This transition point coincides with the transition between the Regime I and Regime II of the stress-optical behavior, as indicated in the figure.

4. Structural interpretation

The focus of this study was to investigate the influence of non-linear deformation rate profile on the development of structural hierarchy in particular stress-induced crystallization and its implications on long-range network development and thickness uniformity resulting from strain hardening. In addition, the effect of molecular weight, within the available range, was investigated to observe the influence of entanglement density on all the above-mentioned physical phenomenon.

The first question was whether or not one can influence the start of strain-induced crystallization by judicious location of high strain rate segments of deformation profile at low (Logarithmic), intermediate (Sigmoidal) or high (Exponential) profiles. The data clearly point out that the use of Logarithmic profile has the biggest influence on early development of crystallinity that also translates into early development of strain hardening that is directly responsible for the achievement of film uniformity at lower strains. In this mode the use of slower speeds at high strains also helps improve the organization of the crystalline domains by facilitating the partial relaxation of polymer chains that in turn allow them to register with the oriented crystalline domains, facilitating their growth as well as their perfection.

Exponential profile that imparts the highest strain rate at high strains certainly retards the strain-induced crystallization as the early stage of deformation is dominated by the relaxation processes. The delay in the strain-induced crystallization delays the strain hardening allowing for an increased orientation of polymer chains as they are not constrained by the long-range network until high strains are achieved. This in turn allows further development of birefringence. In fact the crystallinity data indicate that the Exponential deformation yields the highest crystallinity for the same total true strain. In other words, the exponential application of strain keeps the structure ''looser'' while the polymer chains become oriented preventing the formation of ''muscle bound'' long-range network at intermediate states thereby facilitating higher strain-induced orientation and consequent crystallinity development at the end of the deformation process.

5. Conclusions

The influence of different types of deformations on the structural development of PET under UCW stretching was investigated. The types of deformation studied included Linear, Sigmoidal, Logarithmic and Exponential deformations. In addition, the effect of M_w was also investigated.

If a uniform thickness profile is desired at lower strains the Logarithmic deformation profile is recommended as it rapidly develops strain-induced crystallization that in turn accelerates the establishment of long-range physical network leading to early strain hardening process. However, to obtain higher crystallinity with higher orientation at the end of deformation, the Exponential deformation profile should be used as it suppresses the early development of long-range physical network formation promoting the delay of crystallinity development to higher strains and leading to high orientation and strain-induced crystallization for the same total strains.

Appendix A

In this appendix the (a) birefringence changes as a function of exponential of true strain (Δn vs $\exp(\varepsilon)$) and the (b) birefringence changes as a function of exponential of the double of the true strain (Δn vs $\exp(2\varepsilon)$) are presented for PET (Fig. 24).

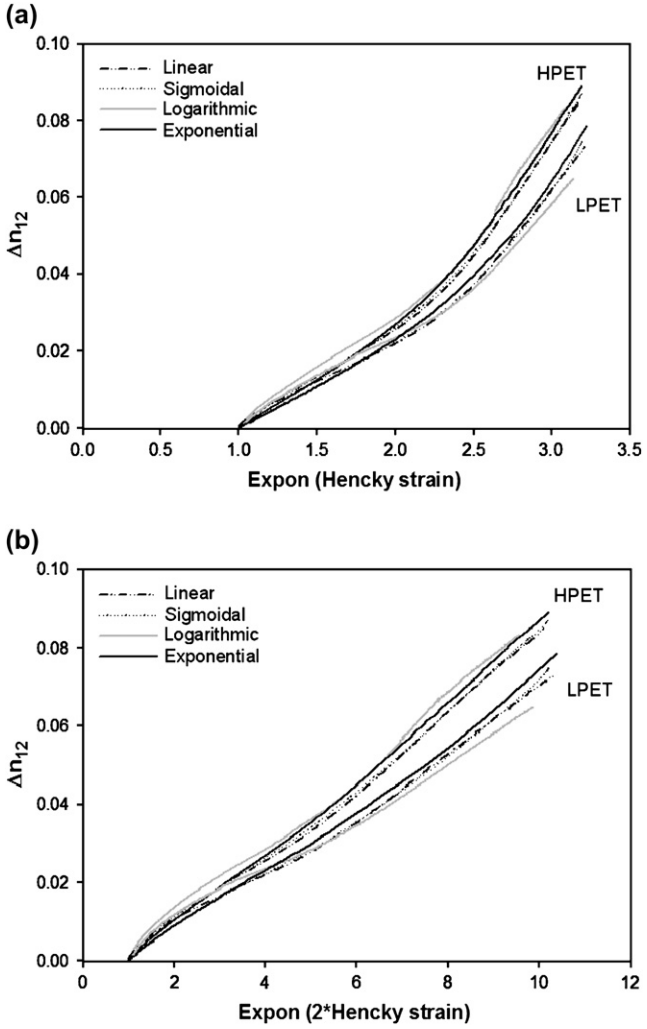

Fig. 24. Strain optical behavior of PET as a function of (a) exp (Hencky strain) and (b) exp (2*Hencky strain) for low and high M_W PET for all types of deformation used.

References

[1] Cakmak M, White JL, Spruiell JE. Journal of Polymer Engineering 1986; 6:1–4.
[2] Cakmak M, White JL, Spruiell JE. Polymer Engineering and Science 1987;27:893.
[3] Wu JP, White JL, Cakmak M. Colloid and Polymer Science 1989; 267(10):881–8.
[4] Kang HJ, White JL, Cakmak M. International Polymer Processing 1990; 5(1):62–73.
[5] Venkatesvaran H, Cakmak M. Polymer Engineering and Science 2001; 41(2):341–57.
[6] Iwakura K, Wang YD, Cakmak M. International Polymer Processing 1992;7(4):327–33.
[7] Marco Y, Chevalier L, Regnier G, Poitou A. Macromolecular Symposia 2002;185:15–34.
[8] Nakayama K, Qi K. Polymers and Polymer Composites 2000;8(6): 387–93.
[9] Hegemann B, Kech A, Goschel U, Belina K, Eyerer P. Journal of Macromolecular Science Part B Physics 2002;41(4–6):647–56.
[10] Blundell DJ, MacKerron DH, Fuller W, Mahendrasingam A, Martin C, Oldman RJ, et al. Polymer 1996;37(15):3303–11.
[11] Blundell DJ, Oldman RJ, Fuller W, Mahendrasingam A, Martin C, MacKerron DH, et al. Polymer Bulletin (Berlin) 1999;42(3): 357–63.
[12] Mahendrasingam A, Martin C, Fuller W, Blundell DJ, Oldman RJ, MacKerron DH, et al. Polymer 2000;41:1217–21.
[13] Sen TZ, Toki S, Cakmak M. In: 59th annual technical conference – society of plastic engineers, vol. 2; 2001. p. 1510–4.
[14] Taner SZ. PhD dissertation, University of Akron, Akron, OH, USA; 2003.
[15] Hassan M. PhD dissertation, University of Akron, Akron, OH, USA; 2004.
[16] Middleton AC, Duckett RA, Ward IM, Mahendrasingam A, Martin C. Journal of Applied Polymer Science 2001;79(10):1825–37.
[17] Salem DR. Polymer 1992;33(15):3182–8.
[18] Salem DR. Polymer 1992;33(15):3189–92.
[19] Gorlier E, Haudin JM, Billon N. Polymer 2001;42:9541–9.
[20] Mahendrasingam A, Martin C, Fuller W, Blundell DJ, Oldman RJ, Harvie JL, et al. Polymer 1999;40:5553–65.
[21] Blundell DJ, Mahendrasingam A, Martin C, Fuller W, MacKerron DH, Harvie JL, et al. Polymer 2000;41(21):7793–802.
[22] Mahendrasingam A, Blundell DJ, Martin C, Fuller W, MacKerron DH, Harvie JL, et al. Polymer 2000;41:7803–14.
[23] Kawakami D, Ran S, Sics I, Avila-Orta C, Chu B, Hsiao BS. Polymeric Materials Science and Engineering 2003;89:712–3.
[24] Kawakami D, Hsiao BS, Ran S, Burger C, Fu B, Sics I, et al. Polymer 2004;45:905–18.
[25] Ran S, Wang Z, Burger C, Chu B, Hsiao BS. Macromolecules 2002; 35(27):10102–7.
[26] Jakeways R, Klein JL, Ward IM. Polymer 1996;37(16):3761–2.
[27] Carr PL, Timothy MN, Ward IM. Polymers for Advanced Technologies 1997;8:592–600.
[28] Gutierrez MCG, Karger-Kocsis J, Riekel C. Macromolecules 2002;35: 7320–5.
[29] Blundell DJ, Mahendrasingam A, Martin C, Fuller W. Journal of Materials Science 2000;35:5057–63.
[30] Welsh GE, Blundell DJ, Windle AH. Journal of Materials Science 2000; 35:5225–40.
[31] Ward IM, Bleackley M, Taylor DJR, Cail JI, Stepto RFT. Polymer Engineering and Science 1999;39(12):2335–48.
[32] Hassan M, Cakmak M. In: 62nd annual technical conference – society of plastic engineers, vol. 2; 2004. p. 2127–9.
[33] Ito H, Suzuki K, Kikutani T, Nakayama K. In: PPS 18th conference proceedings, Portugal; 2002.
[34] Ryu DS, Inoue T, Osaki K. Polymer 1998;39(12):2515–20.
[35] Ajji A, Cole KC, Dumoulin MM, Brisson J. Polymer 1995;36(21): 4023–30.
[36] Le Bourvellec G, Monnerie L, Jarry JP. Polymer 1986;27(6):856–60.
[37] Gorlier E, Agassant J-F, Haudin J-M, Billon N. Plastics, Rubber and Composites 2001;30(2):48–55.
[38] Le Bourvellec G, Beautemps JJ. Journal of Polymer Science 1990;39(2): 319–28.
[39] Stein RS. Journal of Polymer Science 1957;14:383.
[40] Guan J, Wang L, Poter R. Journal of Polymer Science Part B Polymer Physics 1992;30:687.
[41] Kanai T. In: Kanai T, Campbel GA, editors. Film Processing. Munich: Hanser Publishers, ISBN 1-56990-252-6; 1999.
[42] Campbell GA, Cao B, Babel AK. In: Kanai T, Campbel GA, editors. Film processing. Munich: Hanser Publishers, ISBN 1-56990-252-6; 1999.
[43] Yamada T. In: Kanai T, Campbel GA, editors. Film processing. Munich: Hanser Publishers, ISBN 1-56990-252-6; 1999.
[44] Lapersonne P, Tassin JF, Monnerie L. Polymer 1994;35(10):2192–6.
[45] Cakmak M. Processing. In: Kanai T, Campbel GA, editors. Munich: Hanser Publishers, ISBN 1-56990-252-6; 1999.
[46] Inoue T, Matsui H, Murakami S, Kohjiya S, Osaki K. Polymer 1997;38:5.
[47] Ito H, Suzuki T, Kikutani T. In: 45th annual technical conference – society of plastic engineers, vol. 2; 1999. p. 1715.
[48] Ajji A, Zhang X. Macromolecular Symposia 2002;185:3–14.
[49] Mulligan J. PhD dissertation, University of Akron, Akron, OH, USA; 2004.